Energy Conversion and Management 111 (2016) 299–314

Contents lists available at ScienceDirect

Energy Conversion and Management

journal homepage: www.elsevier.com/locate/enconman

Model predictive control-based efficient energy recovery control strategy for regenerative braking system of hybrid electric bus

Liang Li [a,b], Yuanbo Zhang [a], Chao Yang [a,*], Bingjie Yan [a], C. Marina Martinez [c]

[a] The State Key Laboratory of Automotive Safety and Energy, Tsinghua University, Beijing 100084, China
[b] Collaborative Innovation Center of Electric Vehicles in Beijing, Beijing 100084, China
[c] Centre of Automotive Engineering, Cranfield University, MK43 0AL, UK

ARTICLE INFO

Article history:
Received 2 September 2015
Accepted 20 December 2015

Keywords:
Energy recovery control
Modified nonlinear model predictive control
Regenerative braking system
Hybrid electric bus
Optimization algorithm

ABSTRACT

As one of the main working modes, the energy recovered with regenerative braking system provides an effective approach so as to greatly improve fuel economy of hybrid electric bus. However, it is still a challenging issue to ensure braking stability while maximizing braking energy recovery. To solve this problem, an efficient energy recovery control strategy is proposed based on the modified nonlinear model predictive control method. Firstly, combined with the characteristics of the compound braking process of single-shaft parallel hybrid electric bus, a 7 degrees of freedom model of the vehicle longitudinal dynamics is built. Secondly, considering nonlinear characteristic of the vehicle model and the efficiency of regenerative braking system, the particle swarm optimization algorithm within the modified nonlinear model predictive control is adopted to optimize the torque distribution between regenerative braking system and pneumatic braking system at the wheels. So as to reduce the computational time of modified nonlinear model predictive control, a nearest point method is employed during the braking process. Finally, the simulation and hardware-in-loop test are carried out on road conditions with different tire–road adhesion coefficients, and the proposed control strategy is verified by comparing it with the conventional control method employed in the baseline vehicle controller. The simulation and hardware-in-loop test results show that the proposed strategy can ensure vehicle safety during emergency braking situation and improve the recovery energy almost 17% compared with the conventional rule-based strategy in the general braking situation. Therefore, the proposed control strategy might offer a theoretical reference for the design of the actual braking controller in engineering practice.

1. Introduction

The energy depletion and environment pollution have always been the problems hindering the rapid development of the automotive industry. Hybrid electric vehicle (HEV) technology might be the primary solution, due to its characteristics of better fuel economy and lower exhaust emissions in comparison to conventional vehicles [1]. Within the fast expansion of HEV technology, its application to the area of urban buses has made great progress [2]. Among various configurations of HEV, single-shaft parallel powertrain with the automatic mechanical transmission (AMT) have attracted more and more attention due to its compact structure and transmission efficiency [3]. Braking energy recovery is an important working mode for improving fuel consumption and reduce pollutant emissions in HEV. A research about the potential of this technique shows that from one third to one half of the driving energy is dissipated during braking in urban driving circles [4]. Regenerative braking control strategies included series and parallel types. In the Parallel strategy, the friction braking system is the same as in conventional vehicles, and the regenerative torque is added into the friction braking system proportionately. In the series strategy, the friction braking torque can be modulated, and the overall braking torque is controlled to meet the driver demand.

In order to get more efficiency and better capacity of the regenerative braking energy, the existing research has focused on the series strategy. Using this configuration, the regenerated energy is mainly limited by three constrains [5]. First, the regenerative torque depends on the maximum braking torque provided by the motor, which is designed for high torque and power density [6]. Second, the regenerative power is limited by the charging power capability of the battery [7]. To avoid the over-charging or over-discharging and provide a powerful guarantee for the optimization of HEV, the battery's power characteristic should be considered in

* Corresponding author.
E-mail address: yc19861029@126.com (C. Yang).

http://dx.doi.org/10.1016/j.enconman.2015.12.077
0196-8904/

Nomenclature

A	vehicle frontal area (m^2)
a_1	acceleration of vehicle (m/s^2)
b	longitudinal distance from rear wheel to the center of gravity of vehicle (m)
C_D	aerodynamic drag coefficient (–)
e_i	difference of the desired vehicle speed and the predictive vehicle speed (m/s)
$\tilde{e}$	difference of v_{mod} and v_{act} (m/s)
F_{resist}	total resist force (N)
F_w	wind resist force (N)
F_{z1}, F_{z2}	perpendicular force of the front and rear wheels respectively (N)
h_c	control horizon (–)
h_p	prediction horizon (–)
$\tilde{i}$	corresponding output of the set W and W_v (–)
J_1, J_2	moments of inertia of the front, rear wheels respectively ($kg\ m^2$)
K_{b1}, K_{b2}	stiffness for the front wheel and rear wheel respectively (kN/m)
k_{pb}	the ratio coefficient between the pneumatic braking torque and the braking pressure (–)
m	overall mass of vehicle (kg)
m_s	sprung mass of vehicle (kg)
p	pneumatic pressure in the braking chamber (MPa)
p_{ij}	optimal position of the particle in its history (–)
R_1, R_2	radius of the vehicle wheel (m)
r	variation factor (–)
s_i	slip ratio of the wheels (–)
T_{b1}, T_{b2}	pneumatic braking torque on the front and rear wheel (N m)
$T_{pchange,\max}$	maximum braking torque change rate of the pneumatic braking system (N m)
$T_{rechange,\max}$	maximum braking torque change rate of the motor (N m)
Ts	sample time adopted in the model prediction (s)
u_{cont}	output of the controller (–)
u_{hold}	change rate in the pressure hold phase (MPa/s)
$u_{ij}(t+1)$	position of the particle in new generation (–)
u_x	change rate of braking pressure (MPa/s)
v	vehicle speed (m/s)
v_{mod}	modified vehicle speed using the feedback method (m/s)
v_{pre}	vehicle speed based on the predictive model (m/s)
W	a compact subset of the domain of the controller inputs (–)
w_a, w_b, w_c	weight factor for the inertia velocity, velocity to go to the optimal value of the particle in the history, velocity to go to the optimal combination respectively (–)
$\tilde{w}$	factors in W_v (–)
X	current vehicle states (–)
Z	vertical motion of vehicle (m)
α_1, α_2	angular acceleration of the front and rear wheel (rad/s^2)
μ_i	friction coefficient (–)
η_i	efficiency of the set of wheel to battery (–)
ω_m	angular velocity of the motor axle (r/min)
τ_0	lag time of the pneumatic braking system (s)
τ_p	time lag coefficient (–)
a	longitudinal distance from the front wheel to the center of the gravity of vehicle (m)
B,C,D,E	coefficients of the magic formula (–)
C_1, C_2	damping coefficients of the front suspension and the rear suspension respectively (kN s/m)
D_0	vertical distance between the center of the gravity of vehicle to the pitching axle (m)
$\bar{e}$	difference of v_{pre} and v_{act} (m/s)
F_f	roll resist force (N)
F_{s1}, F_{s2}	forces of the suspension on the front wheel and rear wheel (N)
F_{x1}, F_{x2}	the braking force provided by the ground on the front and rear wheels (N)
f_1, f_2	coefficient of roll resist force (–)
h_i	weight factor of the difference in i time step (–)
I_c	battery charging current (A)
J	cost function (–)
J_y	the moment of inertia of the vehicle in the OY direction ($kg\ m^2$)
K_1, K_2	stiffness of the front suspension and rear suspension respectively (kN/m)
l	longitudinal distance from the front wheel to rear wheel (m)
m_1, m_2	mass of the front wheel and rear wheel respectively (kg)
$P_{batt\_\lim}$	maximum charging power of battery (W)
p_{gi}	position in the optimal combination (–)
p_t	target braking pressure (MPa)
R_{int}	Initial resistance of battery (Ω)
S_{xrefer}	desired slip ratio (–)
T_b	pneumatic braking torque (N m)
T_{change}	change rate limits for the particle (N m)
T_{reb}	regenerative braking torque (N m)
$Tb_{re,\max}$	maximum braking torque the motor can provide (N m)
U_c	battery charging voltage (V)
u_{dec}	change rate of the braking pressure reduction (MPa/s)
$u_{ij}(t)$	position of the particle in previous generation (–)
$u_{Inc.}$	change rate when the braking pressure increasing (MPa/s)
V_{oc}	the battery open-circuit voltage (V)
v_{act}	actual vehicle speed (m/s)
v_{ij}	velocity of particle (–)
v_{ref}	desired vehicle speed (m/s)
W_v	a set of finite point which is the set, W (–)
w_x, w_y, w_z	weight factors that denote the important level of the vehicle speed tracking performance, the braking energy recovery efficiency, the vehicle safety performance respectively (–)
$\tilde{w}^{NP}$	the nearest point (–)
x	longitudinal motion of vehicle (m)
Z_1, Z_2	vertical motions of the front wheel and rear wheel respectively (m)
θ	roll angle of sprung mass (°)
η_{motor}	motor efficiency (–)
η_{trans}	transition system efficiency (–)
ω_i	rotation speed of the wheel (rad/s)
τ_x	time taken to reach the target braking pressure (s)
σ	tire–road friction adhesion coefficient (–)

the control strategy [8]. Third, the braking torque is eventually limited by available tire–road friction. Hence, the available regenerative braking torque might not be always large enough to satisfy the braking demand. Consequently, the general braking system of hybrid electric bus (HEB) is composed of both electric regenerative braking system (RBS) and pneumatic friction braking system. During the braking maneuver, the braking torque would be distributed between regenerative braking torque, provided by motor at the rear wheels, and the friction braking torque at the front and rear wheels provided by pneumatic braking system. Considering highly

nonlinear characteristics of the vehicle system and multiple performance objectives, it might be a complex problem to fulfill the efficient energy recovery while ensuring the vehicle braking stability.

Several rule-based regenerative braking strategies, which are commonly used in engineering practice, have been proposed in recent years. For the rear-driven electrified vehicle, a modified control strategy is proposed to improve the recovery efficiency by Zhang [9]. An electronically controlled braking system is proposed to simultaneously control regenerative and mechanical braking force developed by Gao [10]. An integrated control strategy coordinating regenerative and pneumatic braking force is designed and applied in the fuel cell hybrid electric bus [11]. So as to keep small fluctuation of the total frictional and regenerative braking force during the braking modes transition, a coordinated controller is designed for the pneumatic braking system to compensate for the motor error [12].

Moreover, some other strategies based on control and optimization technologies, have also been presented to control the hybrid braking system. Kang present a coordinated cascade control method using two sliding-mode controllers, so as to deal with the unstable situation when the tire slip ratio exceeds a certain threshold and the vehicle dynamic entered the nonlinear region on the friction road surfaces [13]. Furthermore, a sliding-mode controller which decides how to distribute the braking force between the regenerative braking and the antilock braking in emergency braking situations is developed to maintain the optimal slip value in [14]. Kanarachos et al. includes an integrated braking controller designed using the state-dependent Riccati equation control technique, for a vehicle driven by an electric motor on the front axle [5]. To recover more braking energy while satisfying the vehicle stability, a genetic algorithm-based control strategy to obtain the optimal brake torque distribution between the regenerative braking and the electrohydraulic brake torque is detailed by Kim in [15]. Fuzzy-logic-based regenerative braking strategies (RBS) integrated with series regenerative braking are explained in [16], so as to present a solution easier for in-vehicle applications. To extend the driving range for electric vehicle, a fuzzy-logic-based regenerative braking strategy, considering the driver's braking force command, vehicle speed, battery SOC and battery temperature, was designed to determine the distribution between the friction braking force and regenerative braking force by Xu [17]. Among all the available methodologies, the nonlinear model predictive method is well-known for its ability to deal with complex optimal control problems as well as to handle nonlinearities and constraints. Huang et al. present a nonlinear model predictive controller for regenerative braking control of lightweight electric vehicles equipped with in-wheel motors [18]. An uncertainty model predictive strategy for the hybrid compound braking control system of an EV with double driving motors is proposed by Liu [19]. Predictive control is also used by Wang et al. along with a robust control law to enhance the robustness with respect to vehicle parameter uncertainties [20].

As evidenced in the literature survey, an efficient energy recovery strategy based on the NMPC for the vehicle pattern of single-shaft parallel hybrid electric bus has not been researched. Firstly, based on the compound braking system of single-shaft parallel HEB, a set of models, including those of the tire, the 7 degrees of freedom (DoF) vehicle dynamic, the electric braking system and the pneumatic braking system, has been built. Then considering the nonlinear characteristic of vehicle and the efficiency characteristic of RBS, the NMPC strategy with particle swarm optimization (PSO) algorithm is adopted to obtain the optimal distribution of the braking torque. In addition, in order to improve the accuracy and optimize the efficiency, several modified algorithms based on the NMPC method with PSO algorithm are considered in the proposed strategy. The computation effort is reduced using the nearest point method. The simulation and hardware-in-loop (HIL) test result show that the proposed control strategy can greatly improve the regeneration efficiency on the condition of ensuring the braking safety of vehicle.

The rest of this paper is organized as follows. In Section 2, the structure of the regenerative braking system of HEB is given and its model is introduced. Section 3 describes the proposed NMPC-based regenerative braking control strategy. Simulation and HIL test results and analyses of the proposed strategy compared with those of conventional control strategy are given in Section 4. This is followed by the concluding remarks in the final section.

2. Model descriptions of RBS

2.1. Regenerative braking system configuration

A single-shaft parallel hybrid electric bus driven by rear axle is used in this paper as platform to design the regenerative braking control method. The vehicle layout is shown in Fig. 1.

As shown in Fig. 1, there are two parts of braking system. One part corresponds to the pneumatic braking system, which is composed of the air compressor, tank, braking valve, modulating valve, pneumatic braking controller, braking pan and pressure sensor between other components. The second part consists of electric braking system, which is mainly composed of battery, inverter, motor and AMT.

The system is divided into three levels gathering each part mentioned above. The vehicle controller is put in the highest level, which contains the integrated braking control strategy. The second level contains the pneumatic braking controller, the electric controller and the AMT controller in the electric braking system, whose main task is to coordinate regenerative and pneumatic braking torque. Electric and pneumatic braking system without controller are included in the third level, whose task is to realize the braking process under the controller's supervision. In the pneumatic braking system, the pressure adjustment at the wheel master cylinder can be achieved by modulating valves and Fig. 1 shows that every wheel is equipped with the modulating valves, so that each wheel can be controlled by the pneumatic braking controller independently.

2.2. RBS model

Vehicle dynamics model, tire model, electric braking system model, pneumatic braking system model et al. are detailed in this section by taking authorized articles as references. These are used to verify the performance of regenerative braking control strategy through model simulation.

2.2.1. Vehicle dynamics model

The 7 DoF model of vehicle dynamics is built considering load transfer, as shown in Fig. 2.

The OXYZ coordinate system is static relative to the vehicle. OX represents the longitudinal direction of the vehicle, which points forwards, and OZ is perpendicular to the ground, OY is perpendicular to the OXZ plane. The 7 DoF of the vehicle model are as follows: longitudinal motion freedom represented by X, vertical motion freedom represented by Z, roll angle of the sprung mass denoted by θ, vertical motion of the front wheel denoted by Z_1, rotation speed of the front wheels represented by the rotational speed ω_1, vertical motion of the rear wheel denoted by Z_2, and rotation speed of the rear wheels represented by the rotational speed ω_2.

According the vehicle dynamics equations, the longitudinal force equations are given by:

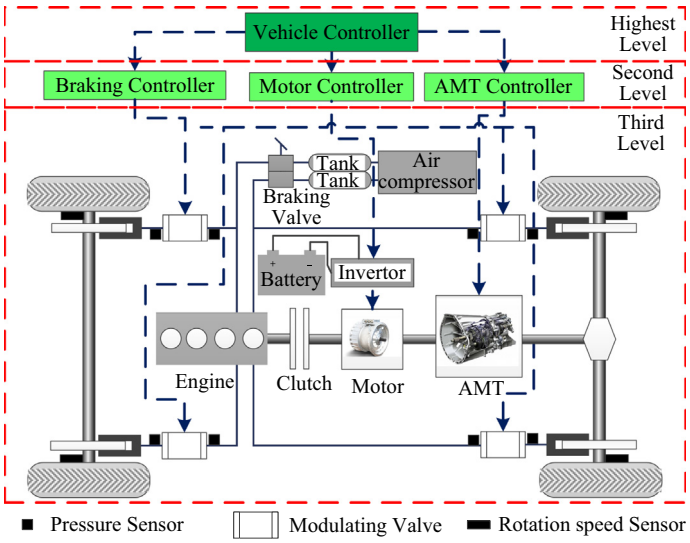

Fig. 1. The configuration of RBS.

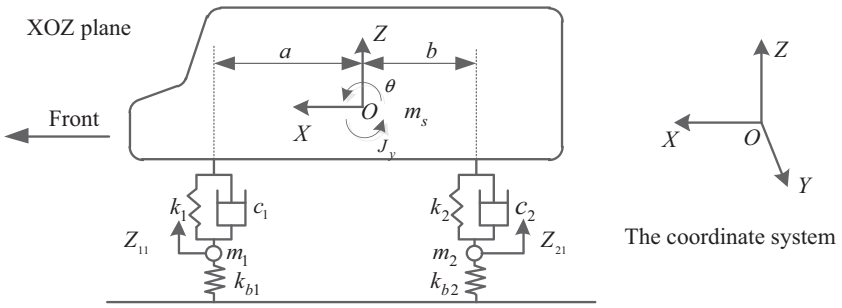

Fig. 2. The schematic diagram of longitudinal vehicle dynamics.

$$\frac{1}{2}m\ddot{x}+\frac{1}{2}m_sD_0\ddot{\theta}=F_{x1}+F_{x2}-F_{resist} \tag{1}$$

$$F_{resist}=F_f+F_w \tag{2}$$

$$F_f=mg(f_1+f_2\dot{x}) \tag{3}$$

$$F_w=\frac{C_DA\dot{x}^2}{21.15} \tag{4}$$

The sprung mass motion is described by:

$$m_s\ddot{Z}+F_{s1}+F_{s2}=0 \tag{5}$$

$$\frac{1}{2}J_y\ddot{\theta}-\frac{1}{2}m_sD_0\ddot{x}-F_{s1}a+F_{s2}b=0 \tag{6}$$

The perpendicular wheel forces by:

$$m_1\ddot{Z}_1-F_{s1}+K_{b1}Z_1=0 \tag{7}$$

$$m_2\ddot{Z}_2-F_{s2}+K_{b2}Z_2=0 \tag{8}$$

The wheel rotation motion by:

$$J_1\dot{\omega}_1=F_{x1}R_1-T_{b1} \tag{9}$$

$$J_2\dot{\omega}_2=F_{x2}R_2-T_{b2}-T_{reb} \tag{10}$$

The wheel perpendicular force by:

$$F_{z1}=m_sgb/2l+m_1g-K_{b1}Z_1 \tag{11}$$

$$F_{z2}=m_sga/2l+m_2g-K_{b2}Z_2 \tag{12}$$

The suspension forces are given by:

$$F_{s1}=K_1(Z-Z_1-a\theta)+C_1(\dot{Z}-\dot{Z}_1-a\dot{\theta}) \tag{13}$$

$$F_{s2}=K_2(Z-Z_2+b\theta)+C_2(\dot{Z}-\dot{Z}_2+b\dot{\theta}) \tag{14}$$

where m is the overall mass of vehicle, m_s is the sprung mass of vehicle. Z_1, Z_2 are the vertical motions of the front wheel and the rear wheel respectively. m_1, m_2 are the mass of the front wheel and the rear wheel respectively. F_{s1} denotes the force of the suspension on the front wheel. F_{s2} denotes the force of the suspension on the rear wheel. F_{Z1}, F_{Z2} are the perpendicular force of the front and rear wheels respectively. F_{x1}, F_{x2} are the braking force provided by the ground on the front and rear wheels. J_y is the moment of inertia of the vehicle in the OY direction. J_1, J_2 are the moments of inertia of the front, rear wheels respectively. R_1, R_2 are the radius of the front, rear wheels respectively. a is the longitudinal distance from the front wheel to the center of gravity of the vehicle. b is the longitudinal distance from the rear wheel to the center of gravity of the vehicle. l is the longitudinal distance from the front wheel to the rear wheel. D_0 is the vertical distance between the center of gravity of the vehicle to the pitching axle. K_{b1}, K_{b2} are the stiffness for the front wheel and rear wheel respectively. K_1, K_2 are the stiffness of the front suspension and the rear suspension respectively. C_1, C_2 are the damping coefficients of the front suspension and the rear suspension respectively. F_{resist}, F_f, F_w are the total resist force, the roll resist force, and the wind resist force respectively. And the road is assumed to be plane, thus the gradient resist force is assumed to be zero. f_1, f_2 denote the coefficient of the roll resist force. C_D is the aerodynamic drag coefficient. A is the vehicle frontal area. T_{b1}, T_{b2} are the pneumatic braking torque on the front and rear wheel respectively. T_{reb} is regenerative braking torque.

2.2.2. Tire model

In the RBS, the tire model serves as the bridge connecting the system inputs (front pneumatic braking torque, rear pneumatic

braking torque and regenerative braking torque) with the system states, including longitudinal and vertical motion. Several candidate tire models can be selected for this problem, including empirical and analytical options [21]. In this paper, the empirical model 'magic formula' is selected given its suitability for tire behavior simulation, and the fact that it does not increase the system number of states. The equations of the magic formula tire model are shown as follows:

$$\mu_i = \sigma D \sin(C \tan^{-1}\{BS_{xi} - E[BS_{xi} - \tan^{-1}(BS_{xi})]\}) \quad (15)$$

$$S_{xi} = \frac{\omega_i R_i - v}{v} \quad (16)$$

$$F_{xi} = \mu_i F_{Zi}\ i \in \{1,2\} \quad (17)$$

where μ is the friction coefficient, which is dependent on the longitudinal slip radio s and the tire–road friction adhesion coefficient σ.

The meanings of parameters B, C, D and E can be found in [22], which are mostly related to the tire properties, assumed to be known. The braking force generated at the ground is strongly influenced by the different tire–road friction adhesion coefficients. The tire–road friction adhesion coefficient can be as low as 0.1–0.3 on the icy roads and as high as 0.6–0.8 on the dry asphalt roads. The tire–road friction adhesion coefficient recognition method can be found in [13]. The relationship between friction adhesion coefficient, longitudinal slip ratio and tire–road friction adhesion coefficient is shown in Fig. 3. When the slip ratio is 0.2, the ratio between F_x and F_z reaches its top, and when the slip ratio in the region of −0.1 to 0.1, the relation between slip ratio and ratio between F_x and F_z is approximately linear. In case the slip ratio is out of the region, the relation shows high nonlinear characteristic.

2.2.3. Electric braking system

The electric braking system model includes battery model and motor model.

2.2.3.1. Battery model. The battery model is based on the Li-Ion battery of a General Motors electric vehicle in ADVISOR. As shown in Fig. 4, the battery model is simplified as an internal resistance model, which was described in [23]. V_{oc} is the open-circuit voltage, R_{int} is the internal resistance, U_c, I_c denote the battery charging voltage and current respectively in Fig. 4. And the battery actual capacity, whose maximum is 80 A h, is related to the previous SOC and the temperature data. And the internal resistance of the battery, is related to the previous SOC and the temperature data too.

2.2.3.2. Motor model. The permanent magnet motor is selected in this paper, the parameters of motor is shown as follows: the max torque is 750 N m; the nominal power is 94 kW; the peak power is 121 kW.

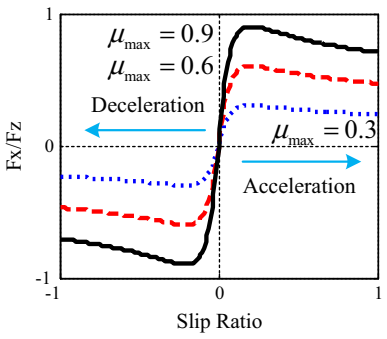

Fig. 3. The relationship of slip ratio and friction adhesion coefficient.

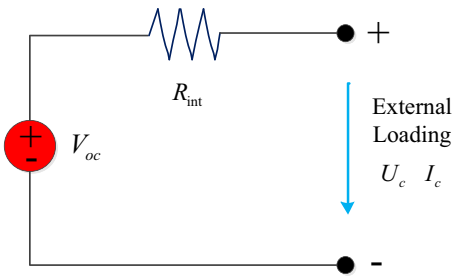

Fig. 4. The internal resistance model of battery.

The motor efficiency in the RBS has been taken into consideration, which can be denoted by the following equation:

$$\eta_{motor} = \frac{U_c I_c}{T_{reb}\omega_m} \quad (18)$$

where ω_m is the angular velocity of the motor axle. η_{motor} is the motor efficiency.

The motor efficiency map is used to calculate the optimal regenerative braking torque by the controller. As depicted in Fig. 5, the blue thick lines denotes the maximum torque that the motor can provide, the contours of different colors are denote the efficiency of motor in the special working area. Provided that the wheel speed is given, the optimal regenerative braking torque which can recapture the most braking energy, can be obtained. Besides, the motor is only active when its rotational speed is higher than 200 r/min, which is the internal logic in the motor controller for the safety consideration.

2.2.4. Pneumatic braking system model

The pneumatic braking system construction has been shown in Fig. 1. The pressure provided by the air compressor and the braking pressure in the braking chamber can be controlled by the modulating valve, which is operated by the braking controller command [13]. In practice, the relationship between the time and the active braking pressure might be simplified as shown in Fig. 6. The percentage values (20%, 60%, 100%) are denote the opening degree of modulating solenoid valve. When the target pressure p_t is demanded, the real braking pressure does not increase at the beginning and then raises linearly, due to the response time of the pneumatic system. The change rate is different depending on the modulating valve characteristics. The time response to reach the target braking pressure might be expressed as follows:

$$\tau_x = \frac{p_t}{u_x} + \tau_0 \quad (19)$$

where p_t is the target brake pressure and u_x is the change rate of braking pressure, τ_0 is the lag time of the pneumatic braking system. The pneumatic brake model may be simplified as a first-

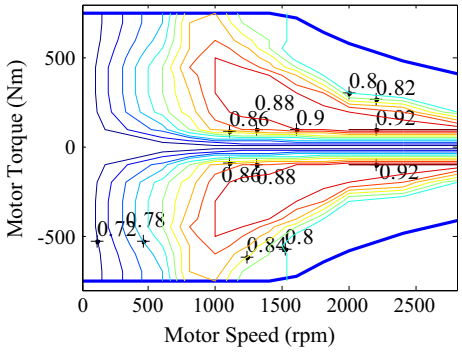

Fig. 5. Motor efficiency.

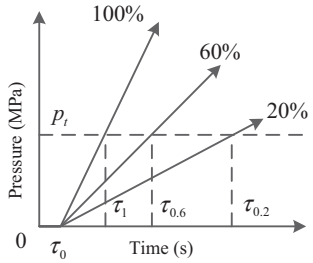

Fig. 6. The characteristics of pneumatic braking system.

order integration model as shown in Fig. 7 [17], where $u_{Inc.}$ is the change rate when the braking pressure increase, u_{dec} is the rate of the braking pressure reduction and u_{hold} is zero in the pressure hold phase. τ_p is the time lag coefficient.

The relationship between the braking pressure and the braking torque might be expressed as follows:

$$T_b = k_{pb}p \tag{20}$$

As mentioned above, T_b is the pneumatic braking torque applied on the wheel and p is the pneumatic pressure in the braking chamber. The ratio k_{pb} can be calibrated according to the value obtained by repeated braking test of the HEB.

The parameters in the simulation model are shown in Table 1.

Table 1
Parameters in the simulation model.

Parameters	Unit	Value	Parameters	Unit	Value
A	m^2	8.46	B	–	8.98
C	–	1.62	C_1, C_2	kN s/m	30
C_D	$N s^2/m^2$	0.51	D	–	1
D_0	m	0.1545	E	–	0.5
J_1, J_2	kg m^2	14	J_y	kgm^2	70,875
K_1, K_2	kN/m	700	K_{b1}, K_{b2}	kN/m	980
R_1, R_2	m	0.48	Ts	ms	10
a	m	3.06	b	m	2.04
f_1	–	0.0076	f_2	–	5.6×10^{-5}
g	m/s^2	9.81	h	m	1
l	m	5.1	m	kg	14,000
m_s	kg	13,180	m_1, m_2	kg	67
$u_{Inc.}$	MPa/s	5	u_{dec}	MPa/s	5
τ_p	–	0.01	k_{pb}	–	20,000

3. Regenerative braking control strategy

Considering the nonlinear characteristic of the RBS system and the multi-objective characteristic of the braking process, NMPC method might be adopted to improve the recovery energy whilst ensuring the vehicle braking safety. The proposed NMPC regenerative braking strategy can accommodate the forecasting errors by combining real-time observation and short-term prediction. NMPC determines the series of optimal control sequences over a receding finite horizon. The PSO is well known for its ability to solve multi-factor and nonlinear optimization problem [24]. Due to the meta-heuristic nature and simple implementation characteristic, PSO method have found a wide range of application in many domains of computer, science and applied mathematics [25]. For the high nonlinear and multifactor characteristic of the vehicle dynamic system, the PSO algorithm is adopted in this paper. At each time step, a deterministic optimization problem is solved by the modified PSO method, based on the look-ahead finite-horizon prediction and the updated current state/measurement. However, only the first step of the optimal control sequences is performed, discarding the rest. At each time step, the initial condition over the prediction horizon is determined by the real-time measurement of the actual system. The online optimization process repeats until the braking operation is over.

The desired profile of the vehicle velocity was recognized by several algorithms, as mentioned in [26]. The prediction method of the vehicle velocity can be divided into two groups: one is based on the driving history information; the other is based on the vehicle telemetry such as the Global Positioning System (GPS), the Intelligent Transportation System (ITS) [27]. It is also assumed that the current vehicle states, including vehicle and wheel speed, can be measured by the on-board sensors or evaluated by the mathematical recognition algorithms. The PSO method is employed to calculate the optimal control sequences given its advantage to deal with the nonlinear problem. So as to improve the accuracy and optimal efficiency, several modified algorithms based on the NMPC method combined with PSO algorithm are taken in the proposed strategy. Furthermore, with the aim to reduce the computational effort of the proposed strategy, a nearest point method is employed for the designed control strategy in the braking process.

As shown in Fig. 8, the process of the modified nonlinear model predictive control (MNMPC) strategy includes 5 steps. The detailed process of MNMPC is shown in Table 2.

3.1. The conventional braking control strategy

Recently, many regenerative braking control strategies have been used in engineering practice. One of those has been widely adopted in conventional braking systems and its descriptions is as follows. The desired braking torque is obtained mapping braking pedal position using a look-up table. This torque is distributed between front and rear wheels by a predefined ratio. The regenerative braking torque, provided by the motor, is applied at the rear wheels. In case the regenerative braking torque can satisfy the braking toque demand, all braking torque would be regenerative. However, if the regenerative braking torque cannot satisfied the full torque demand, the motor would provide its max regenerative torque, and the remaining torque would be compensated by the pneumatic braking system.

3.2. MNMPC strategy

3.2.1. Predictive model

In the NMPC strategy, a three DOF vehicle dynamics model is selected to predict the future vehicle states. The three DoF include: vehicle speed v, front wheel rotational speed ω_1 and rear wheel rotational speed ω_2. The load transfer is taken into consideration, but the influence of the sprung system is simplified in this model.

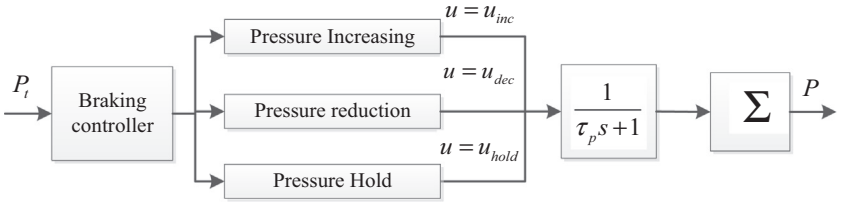

Fig. 7. The model of pneumatic braking system.

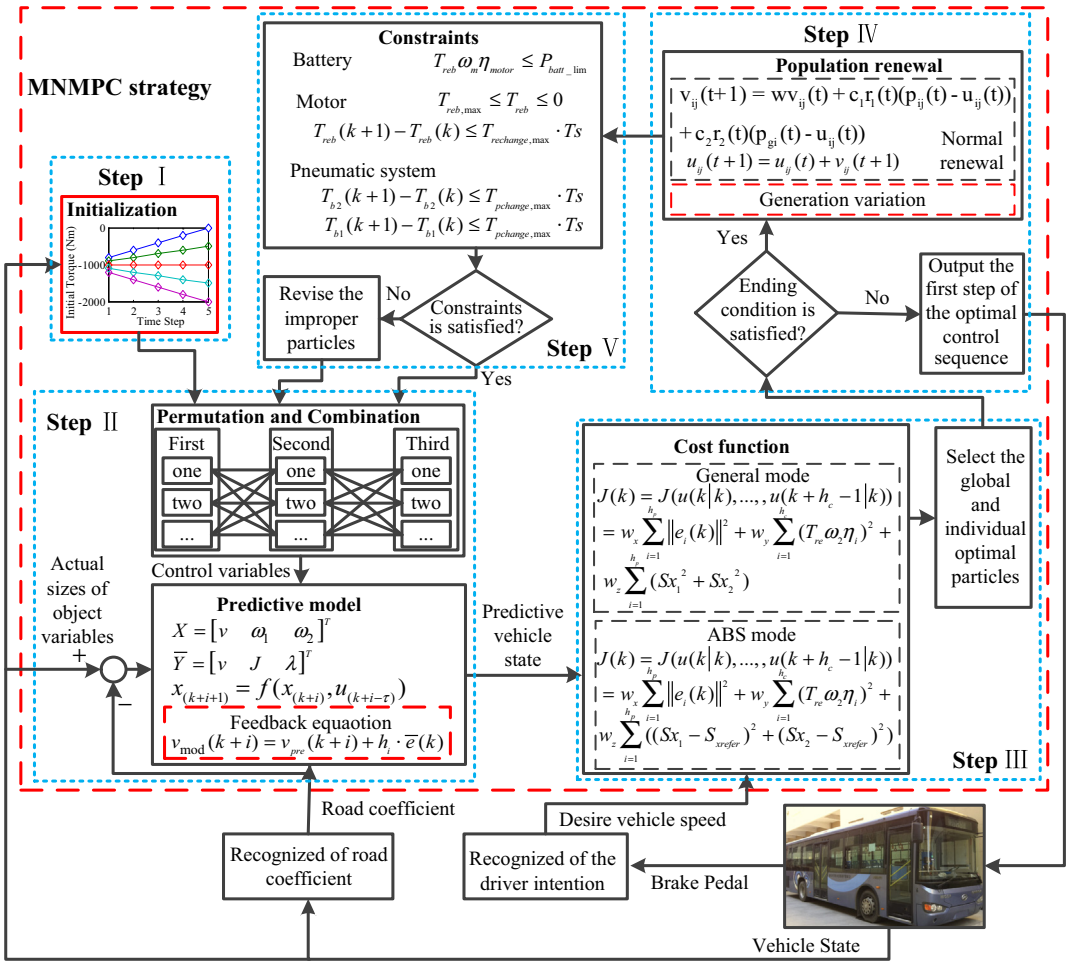

Fig. 8. The NMPC strategy of RBS.

Table 2
Detailed process of NMPC.

Step I	Generate initial population of the control variables with the average initial method. Initialize the PSO parameters, i.e., c_1, c_2, w, and V_{max}
Step II	Take permutation and combination for particles of different control variables, and predict the vehicle states in the prediction horizon for every combination
Step III	Select the optimal combination and select the optimal value of every particle in its history based on the cost function of every combination
Step IV	Judge whether the ending condition is meet, if the answer is yes, the calculation is ended and output the first factor of the optimal sequence of every control variables., if the answer is no, Renew population for the control variables based on the normal renewal method and variation method
Step V	Judge whether the restraint for every particle is meet, if so, jump into step II. In addition, if the value is over the range of the restraint, Renew the value of the particle randomly in the boundary of the restraint

Thus, the discrete-time form of the predictive model can be derived as follows:

$$ma_1(k) = F_{x1}(k) + F_{x2}(k) - F_{resist}(k) \tag{21}$$
$$v(k+1) = v(k) + a_1(k)Ts \tag{22}$$
$$\alpha_1(k) = (T_{b1}(k) - R_1F_{x1}(k))/J_1 \tag{23}$$
$$\omega_1(k+1) = \omega_1(k) + \alpha_1(k)Ts \tag{24}$$
$$\alpha_2(k) = (T_{b2}(k) + T_{reb} - R_2F_{x2}(k))/J_2 \tag{25}$$
$$\omega_2(k+1) = \omega_2(k) + \alpha_2(k)Ts \tag{26}$$

The variables used in the above equations can be obtained through the following equations:

$$F_{resist}(k) = F_f(k) + F_w \tag{27}$$
$$F_f(k) = mg(f_1 + f_2v(k)) \tag{28}$$
$$F_w(k) = \frac{C_DAv(k)^2}{21.15} \tag{29}$$
$$S_1(k) = (\omega_1(k)R_1 - v(k))/v(k) \tag{30}$$
$$S_2(k) = (\omega_2(k)R_2 - v(k))/v(k) \tag{31}$$
$$\mu_1(k) = \sigma D\sin[C\tan^{-1}(BS_1(k) - E\{BS_1(k) - \tan^{-1}[BS_1(k)]\})] \tag{32}$$
$$\mu_2(k) = \sigma D\sin[C\tan^{-1}(BS_2(k) - E\{BS_2(k) - \tan^{-1}[BS_2(k)]\})] \tag{33}$$
$$F_{Z1}(k) = \frac{mg}{L}\left(b + \frac{a_1(k-1)h}{g}\right) \tag{34}$$
$$F_{Z2}(k) = \frac{mg}{L}\left(a - \frac{a_1(k-1)h}{g}\right) \tag{35}$$
$$F_{x1}(k) = F_{z1}(k)\mu_1(k) \tag{36}$$
$$F_{x2}(k) = F_{z2}(k)\mu_2(k) \tag{37}$$

where k represents the time step. Ts is the sample time adopted in the model prediction. a_1, α_1, α_2 are the acceleration of the vehicle, the angular acceleration of the front wheel and the angular acceleration of the rear wheel respectively. The other variables are mentioned in the second section. The values of the parameters are included in Table 1.

3.2.2. Constraints

Regenerative braking torque in the NMPC is mainly limited by three constraints. The first constraint is the motor physical torque limit, which can be obtained using a look-up table dependent on the motor rotational speed. The second one is the maximum battery charging power. The third constraint corresponds to the charging rate limits imposed by the electric braking system. The pneumatic braking torque in the NMPC is mainly limited by the maximum change rate limits provided by the pneumatic pressure response. The constrains mentioned above can be derived through the following equations:

$$T_{reb}\omega_m\eta_{motor} \leqslant P_{batt\_lim} \tag{38}$$

$$\begin{cases} T_{reb,\max} \leqslant T_{reb} \leqslant 0 \\ T_{reb}(k+1) - T_{reb}(k) \leqslant T_{rechange,\max} \cdot Ts \end{cases} \tag{39}$$

$$T_{b2}(k+1) - T_{b2}(k) \leqslant T_{pchange,\max} \cdot Ts \tag{40}$$

$$T_{b1}(k+1) - T_{b1}(k) \leqslant T_{pchange,\max} \cdot Ts \tag{41}$$

where P_{batt_lim} is the maximum charging power of battery. $T_{reb,\max}$ is the maximum braking torque that the motor can provide. $Tb_{rechange,\max}$ is the maximum braking torque change rate of the motor. $Tb_{pchange,\max}$ is the maximum braking torque change rate of the pneumatic braking system.

3.2.3. Cost function

The vehicle speed tracking performance, energy recovery efficiency and vehicle safety should be considered in the cost function. These objectives are included in a single objective function through weights, which are adapted in different situation. The cost function includes two modes based on the slip ratio of the wheels.

3.2.3.1. General control mode. The general regenerative braking control mode turns on when both slip ratio are lower than a predefined threshold. The main objective in this mode is recovering as much braking energy as possible under the condition that the rear wheel slip ratio is controlled in a reasonable area so as to prevent ABS control intervention. The cost function in this mode is defined as follows:

$$\begin{aligned} J(k) &= J(u(k|k), \ldots, u(k+h_c-1|k)) \\ &= w_x \sum_{i=1}^{h_p} \|e_i(k)\|^2 + w_y \sum_{i=1}^{h_c} (T_{re}\omega_2\eta_i)^2 + w_z \sum_{i=1}^{h_p} (S_1^2 + S_2^2) \end{aligned} \tag{42}$$

where

$$w_z \propto \max(S_1, S_2) \tag{43}$$

$$e_i(k) = v_{ref}(k+i|k) - v(k+i|k) \quad i = 1, \ldots, h_p \tag{44}$$

$$\eta_i = \eta_{trans}\eta_{motor} \quad i = 1, \ldots, h_p \tag{45}$$

where $\|\cdot\|$ is the Euclidean norm. v_{ref} denotes the reference vehicle speed. e_i is difference of the desired vehicle speed and the predictive vehicle speed. h_c is the control horizon. h_p is the prediction horizon. η_i is the efficiency of wheel to battery set. η_{trans} is the transmission system. J is the cost function. w_x, w_y, w_z are weight factors that denote the important level of the vehicle speed tracking performance, the braking energy recovery efficiency, the vehicle safety performance respectively. w_z is a self-adaption factor which value is dependent on the slip ratio. In order to prevent the wheel slip ratio beyond the boundary and turn the ABS control mode on, w_z should be set larger as the slip ratio rise.

3.2.3.2. ABS control mode. The ABS control mode is turned on when any of the front or rear wheels is going to be locked. During ABS control mode, the most important objective is the vehicle safety, which is controlled by keeping the wheel slip ratio within the same range. The cost function is defined as follow:

$$\begin{aligned} J(k) &= J(u(k|k), \ldots, u(k+h_c-1|k)) \\ &= w_x \sum_{i=1}^{h_p} \|e_i(k)\|^2 + w_y \sum_{i=1}^{h_c} (T_{re}\omega_2\eta_i)^2 \\ &\quad + w_z \sum_{i=1}^{h_p} ((S_1 - S_{xrefer})^2 + (S_2 - S_{xrefer})^2) \end{aligned} \tag{46}$$

where S_{xrefer} is the desired slip ratio in the ABS control mode.

3.3. Modified NMPC strategy

Based on the current vehicle state variables and the previous input variables, the PSO algorithm is adopted in the NMPC strategy to look for the optimal control laws at every time step. The modified part of NMPC and PSO strategy mainly include four points, which are shown as follows:

Firstly, to prevent the PSO from reaching a local minimum, the available sets of the control variables have been divided into several even parts. The points of the boundary in every part have been selected in the initial group. For example, if the previous value of the regenerative braking torque is −1000 N m, the change rate is limited by 200 N m every time step. The control horizon is limited to 5 time steps, and the membership of the generation is 5. The initial group of the particles in the PSO for this particular case is shown as Fig. 9. The first particle is on the up boundary of the constraint, the last particle is on the down boundary of the restraint, and the other particles are distributed in the rational area averagely.

Secondly, a variation method in the generation renewal process is used. When a particle is in its renewal process, a statistic value between 0 and 1 is generated at the same time. If this value is smaller than 0.8, the particle is generated by the normal renewal equation. And if this value is greater than 0.8, this particle is randomly generated in the available range under the restraint. The equations can be written as follows:

$$r = rand \tag{47}$$

$$v_{ij}(t+1) = w_a v_{ij}(t) + w_b r_1(t)(p_{ij}(t) - u_{ij}(t)) + w_c r_2(t)(p_{gi}(t) - u_{ij}(t)) \tag{48}$$

$$\begin{cases} u_{ij}(t+1) = u_{ij}(t) + v_{ij}(t+1) & r <= 0.8 \\ u_{ij}(t+1) = u_{ij}(t) + T_{change} - 2rand \cdot T_{change} & r > 0.8 \end{cases} \tag{49}$$

where *rand* is the function that statistic generate a value in the range of 0–1. v_{ij} is the velocity of particle. w, c_1, c_2 are denote the weight factor for the inertia velocity, velocity to go to the optimal value of the particle in the history, velocity to go to the optimal combination respectively. $p_{ij}(t), p_{gi}(t)$ are the optimal value of the particle in its history and optimal combination respectively. $u_{ij}(t)$ is the position of the particle in previous generation and the $u_{ij}(t+1)$ is the position of the particle in new generation. T_{change} is the change rate limits for the particle.

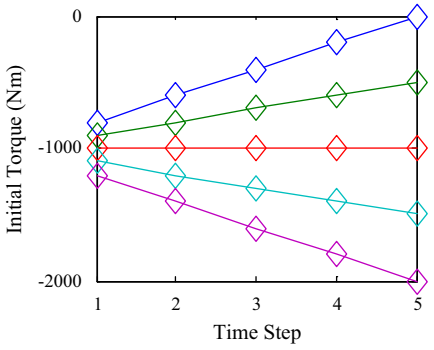

Fig. 9. The initial assumption of control variable.

Thirdly, disturbances surrounding the control variables set a challenge for the PSO algorithm optimization in a limited iteration process. For example, when HEB is running under emergency braking process, the most important performance index is the slip rate, which should be controlled in a certain range to ensure the vehicle safety. All the control variables are included in an integrated particle, generated and renewed as a whole following the traditional PSO method. The optimal particle should be able to control the wheel slip rate at the front wheels, though pneumatic pressure, and rear wheels using pneumatic and regenerative torque control. In order to solve this optimization problem, three control variables are included in different set of particles, which are generated and renewed respectively.

Finally, the RBS controlled with the NMPC strategy becomes a closed-loop system where the control output is based on the current vehicle states. In this paper, another feedback method to modify the predictive vehicle speed is proposed. The equations are detailed as follows:

$$u_{cont} = g(X) \tag{50}$$

$$v_{\mathrm{mod}}(k+i) = v_{pre}(k+i) + h_i \cdot \bar{e}(k) \tag{51}$$

$$\begin{cases} \bar{e}(k) = v_{act}(k) - v_{pre}(k) \\ \tilde{e}(k) = v_{act}(k) - v_{\mathrm{mod}}(k) \end{cases} \tag{52}$$

$$h_1 = \begin{cases} h_1 & \tilde{e}(k) = 0 \\ h_1 - 0.1 & sign(\tilde{e}(k)) \neq sign(\tilde{e}(k-1)) \\ h_1 + 0.1 & sign(\tilde{e}(k)) = sign(\tilde{e}(k-1)) \end{cases} \tag{53}$$

$$h_i = 0.5h_{i-1} \quad i = (1, 2 \ldots, h_p) \tag{54}$$

where X denotes the current vehicle states. u_{cont} is the output of the controller. v_{act} denotes the real vehicle speed. v_{pre} is the vehicle speed based on the predictive model. v_{mod} is the modified vehicle speed using the feedback method. $\bar{e}$ is the difference of v_{pre} and v_{act}. $\tilde{e}$ is the difference of v_{mod} and v_{act}. h_i is the weight factor of the difference. The weight factor h_1 increases if the sign of the current difference is the same as the previous difference sign. In case the signs differ, the weight factor decreases. In addition, the value of h_1 is constraint within 0–1. It should be noted that this feedback method is more effective under constant disturbances.

3.4. Fast implementation of NMPC

The low computation efficiency of NMPC limits its application in real-time control. This problem might be solved using an approximated control function [28]. In particular, the computational burden can be reduced applying the "nearest point" (NP) approach, which is used by Massimo Canale et al. to realize the fast NMPC strategy in [29], approach used in this paper. It should to be noted that using the NP technique for function equivalent is well-assessed in different applications [30].

3.4.1. NP approach

The equivalent function κ^{NP} is computed over a compact subset $W \subset R^n$ of the domain of the exact function κ. It is assumed that the function κ is continuous in W in the NP equivalent, but the optimization result of the PSO method may be not continuous. The function κ can be regarded as a continuous when the PSO results are accurate enough, as the theoretical optimal results are continuous. Inside W, a finite number v of point $\tilde{w}^h, h = 1, \ldots, v$ is suitably chosen, giving rise to the set:

$$W_v = \{\tilde{w}^h \in W, h = 1, \ldots, v\} \tag{55}$$

For each point, the corresponding output $\tilde{i} = \kappa(\tilde{w})$ is off-line computed by the NMPC with PSO method. Then the values of $\tilde{i}, \tilde{w}$ are stored to be used for the on-line computation of NP method.

$$\tilde{i} = \kappa(\tilde{w}), \quad \forall \tilde{w} \in W_v \tag{56}$$

The set W_v is supposed to be chosen such that the following property holds:

$$\lim_{v \to \infty} d_H(W, W_v) = 0 \tag{57}$$

$$d_H(W, W_v) = \sup_{w \in W} \inf_{\tilde{w} \in W_v} (\|w - \tilde{w}\|_2) \tag{58}$$

If the function is continuous, the *Lipschitz* continuous condition should be satisfied, which is denoted as follows:

$$\|\kappa(w^1) - \kappa(w^2)\|_2 \leqslant \gamma \|w^1 - w^2\|_2, \quad \forall w^1, w^2 \in W \tag{59}$$

The equivalent function of NP method is denoted as follows:

$$\tilde{w}^{NP} = \arg \min_{\tilde{w} \in W_v} \|\tilde{w} - w\|_2 \tag{60}$$

$$\kappa^{NP}(w) = \kappa(\tilde{w}^{NP}) \tag{61}$$

where $\tilde{w}^{NP}$ is the nearest point of the real input w. The optimal control variables of w is considered to be the optimal control variables of $\tilde{w}^{NP}$, which has been calculated off-line.

Noted that, the nearest point method set amount of working points, the more the working point set, the more accuracy might be achieved in theory. But the working points need to be burned in the controller, so the number of the points is limited by the memory space of the controller [29]. Therefore, there is a tradeoff between accuracy and the memory space of the controller.

As referred in [28], the following properties are contained in the NP approach:

(1) The restraints of the control variables are always satisfied.
(2) For a given v, a bound ξ^{NP} of the approximated function error can be calculated as follows:

$$\|\kappa(w) - \kappa^{NP}(w)\|_2 \leqslant \xi^{NP} = \gamma d_H(W, W_v), \quad \forall w \in W \tag{62}$$

(3) ξ^{NP} is convergent to zero:

$$\lim_{v \to \infty} \xi^{NP} = 0 \tag{63}$$

It is stated that if the Eqs. (62) and (63) hold, there exists a finite value of v such that the desired performance can be achieved also using the equivalent function. Unfortunately, at present there is no technique to find out a prior number and values of the vector $\tilde{w}$ considered in the off-line computations to guarantee the controller performance. However, it can be realized to estimate the performance of the controller for a given points $\tilde{w}^h$. Thus, in the design of the equivalent controller, an iterative procedure can be employed [28], where the value of v is gradually increased until the desired control objective is achieved.

The procedure of the fast NMPC implementation:

(1) Design the nominal NMPC controller according to the method mentioned above.
(2) Choose the set W_v, and calculate the corresponding output set using the nominal NMPC controller.
(3) Implement the NP control method on-line using the Eqs. (60) and (61).
(4) If needed, tune the set W_v in order to find a satisfactory tradeoff between computational time, memory usage and performance.

3.4.2. Equivalent control strategy for real-time NMPC application

The nominal off-line control strategy used to generate the equivalent control strategy [29] has been performed using a MNMPC algorithm. Considering the memory usage of the actual braking controller, the nominal control law should be simplified.

As shown in Fig. 10, the constraints of the change rate of the pneumatic braking torque are neglected in the NMPC process. The set W_v is composed of five input variables in the simplified NMPC strategy, which are: vehicle speed, front wheel rotation speed, rear wheel rotation speed, desired vehicle speed, and coefficient of the ground, respectively. The vehicle speed set is designed first, defining the other variables based on the vehicle speed.

$$W = [v, \omega_1, \omega_2, v_{ref}, z]^T \in R^5 \tag{64}$$

$$W_v = [0, v_{define} - 10, v_{define} - 10, v_{define} - 10Ts, 0.1]^T \leqslant w \leqslant [90, v_{define} + 1, v_{define} + 1, v_{define} + Ts, 0.9]^T \tag{65}$$

$$\Delta w = [1, 1, 1, Ts, 0.1]^T \tag{66}$$

The control horizon and the prediction horizon are both set to 2. The desired vehicle speed in the equivalent control strategy is set as shown in Table 3. $v_{now}, v_{desired}$ are the input variables for the equivalent control strategy, which are denoted as present vehicle speed and desired vehicle speed two time step later.

Table 3
The desired vehicle speed in the equivalent control strategy.

Time step in the prediction horizon	The desired vehicle speed in the equivalent control strategy
1	$(v_{now} + v_{desired})/2$
2	$v_{desired}$

4. Results and discussion

Simulation and HIL tests are carried out so as to evaluate the safety performance and the energy recovery capability of RBS with the proposed NMPC strategy. This section contains three parts: (1) verification of the vehicle safety performance; (2) verification of the braking energy recovery capability; and (3) HIL test. The detailed results and discussions are given as follows.

4.1. Verification of the vehicle safety performance

The simulation scenario used to verify the vehicle safety performance is set with initial speed equals to 80 km/h, and desired acceleration of −0.6 g. The simulation is carried out on the following surface cases.

Case 1: On the gravel road with a peak equivalent friction parameter of 0.604 and a sliding equivalent friction parameter of 0.557.
Case 2: On the ice road with a peak equivalent friction parameter of 0.306 and a sliding equivalent friction parameter of 0.236.
Case 3: On the μ-jumped road with forward road is the gravel road and rear road is the ice road), ensuring that at least the wheels of one axle may be locked.

4.1.1. The simulation on the gravel road

Vehicle safety is first verified on the gravel road. The simulation results are shown in Fig. 11. It can be seen that there is some difference between the desired speed and the real speed in Fig. 11 (a). There are two main reasons. First, due to the safety objective weight, the desired braking torque cannot be maintained. Second RBS has a response time which introduces certain time delay. In order to maintain the slip ratio within the designed limits and meet both objectives, braking performance and safety, there has to be maintained a difference between vehicle and wheel speed as shown in Fig. 11(b). Fig. 11(c) depicts the wheel split ratio, which is maintained in both cases close to the predefined value 0.15 during the complete braking process. The braking force generated at the ground is shown in Fig. 11(d). Fig. 11(e) shows a small wave response during the last second of the braking event. Provided that no gear-shifting is allowed during ABS control mode, and the motor quit time during emergency braking is faster than that in the general braking situation, this can only be explained due to the difference in quitting time when the motor braking torque is replaced by the pneumatic braking torque. Fig. 11(f) shows the transition between motor driving mode, where the energy recovered is positive and therefore is consumed by the motor, and motor braking mode, when the energy recovery is negative. In Fig. 11(f) the energy recovery is first positive prior to the start of the braking event.

4.1.2. The simulation on the ice road

The results of the emergency braking simulation on the ice road are shown in Fig. 12. There is a large difference between the desired speed and the real speed in Fig. 12(a). The main reason of this phenomenon is that the braking torque provided by the ice ground is too small to satisfy the desired braking torque. As shown in Fig. 12(b), the vehicle speed and the wheel speed curve are similar to the simulation on the gravel road, as well as the slip ratio depicted in Fig. 12(c). The braking force provided by the ice ground is almost half of the braking force provided by the gravel road in Fig. 12(d). Compared with that on gravel road, the proportion of the regenerative braking torque is larger in Fig. 12(e). And the recovery energy on the ice road is merely twice larger than it on the gravel road, as shown in Figs. 12(f) and 11(f). The main reason is that the regenerative braking torque provided by the motor in the simulation on the gravel road and the ice road are almost the same, but the time of regenerative braking on the ice road is much larger than it on the gravel road. As shown in Fig. 12(c), the slip ratios of both the front wheel and the rear wheel are in the desired area, and the vehicle safety performance is ensured.

4.1.3. The simulation on the μ-jumped road

The simulation result on the μ-jumped road is shown as Fig. 13. The road condition is jumped from the grave road to the ice road after 2 s. As depicted in Fig. 13(a), the real speed is close with the desired speed before the jump time, and there is large difference between the desired speed and the real speed after the change instant. The rear wheel speed drops quickly at the jump

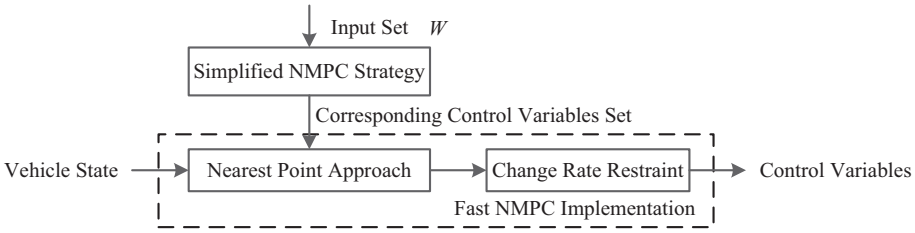

Fig. 10. The structure of the equivalent control strategy.

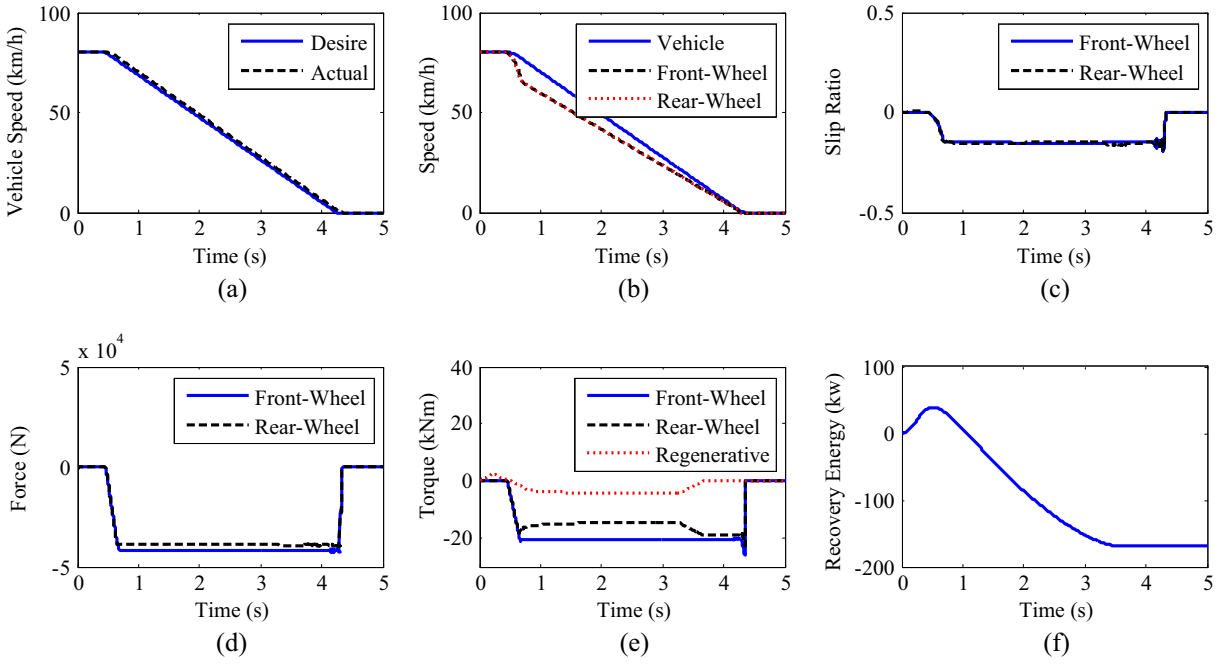

Fig. 11. The simulation result on the gravel road.

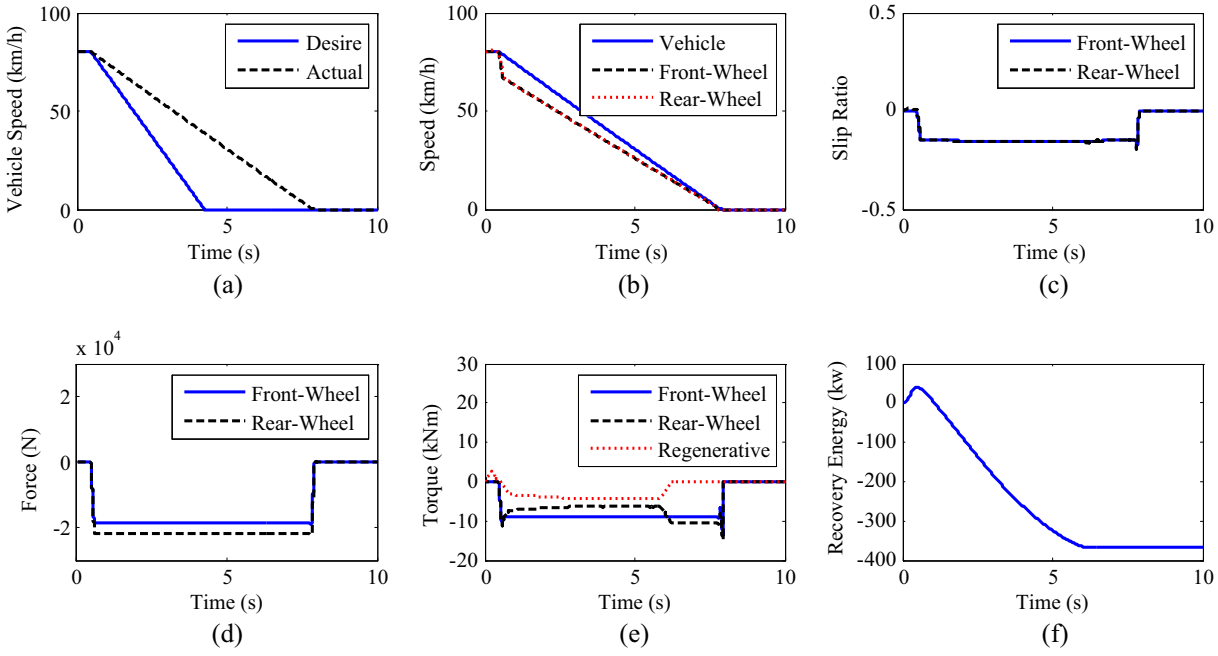

Fig. 12. The simulation result on the ice road.

time in Fig. 13(b). The slip ratio is dropped sharply at the jump time, but none of the wheels are locked and the slip ratio regains its designed range very soon in Fig. 13(c). It shows that the braking force provided by the road fall about half after 2 s in Fig. 13(d). As shown in Fig. 13(e), the regenerative braking torque is reduced to prevent the vehicle from locking the rear wheel at the jump time and retain the maximum braking torque to regenerate more braking energy as the slip ratio is return to the designed range. As it is known, the model predictive method is highly dependent on the accuracy of predictive model, if the parameters in the predictive model do not match, the performance of the control strategy may be difficultly ensured. In the μ-jumped road, the tire–road friction adhesion coefficient changed from 0.6 to 0.3, and the predictive model in the control strategy mismatches with the real world, but the simulation result is acceptable. The main reasons are as follows: first, for the parameters which are crucial and changeful such as the tire–road friction adhesion coefficient, some recognized method may be applied and the parameter in the predictive model may be changed follow with the real world. Second, the proposed NMPC strategy is a closed-loop control method, and the feedback method is employed to ensure the stability performance of the controller. Third, for the parameters which are

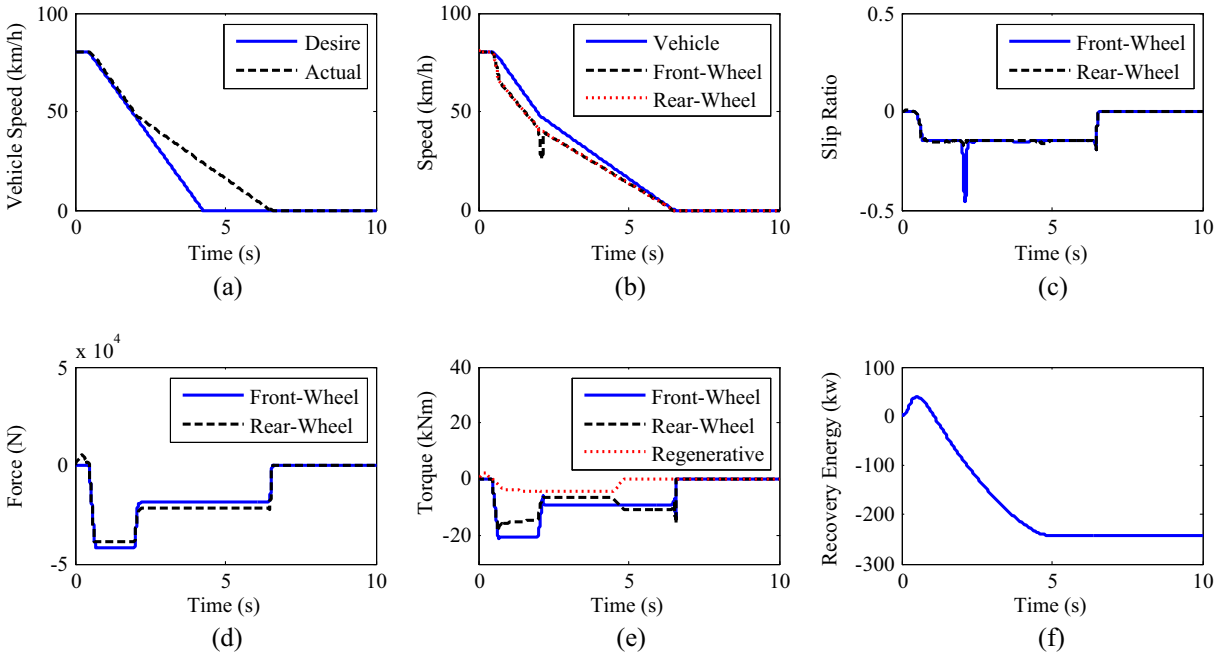

Fig. 13. The simulation result on the μ-jumped road.

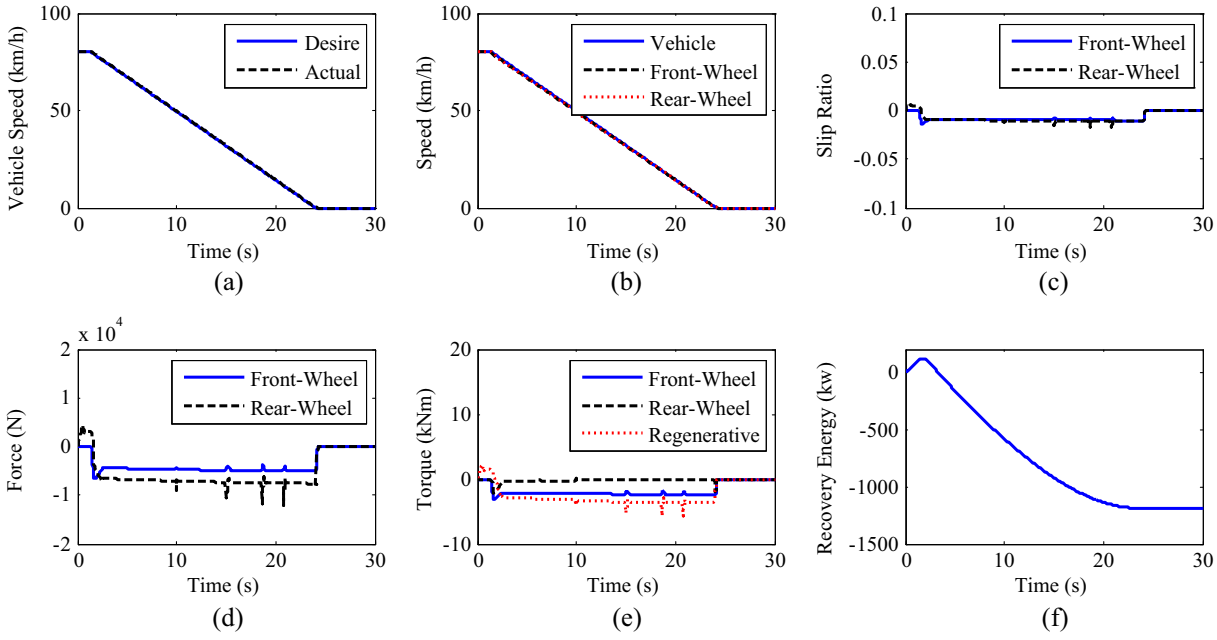

Fig. 14. The simulation result on general condition based on conventional strategy.

changeless, the difference of parameters in the predictive model and the real world would be limited. Therefore, though the performance might be influenced, the stability can also be ensured. It is verified that the proposed regenerative braking NMPC strategy is robust and has the ability to deal with the emergency disturb such as running on the μ –jumped road.

4.2. Verification of the braking energy recovery capability

The scenario of second simulation to evaluate the braking energy recovery capability is designed with initial speed equals to 80 km/h and desired acceleration of −0.1 g, which the vehicle can realized easily. The simulation is taken on the gravel road, the proposed NMPC strategy and the conventional control strategy are employed to control the braking process respectively.

4.2.1. The simulation on the general condition by conventional strategy

The simulation result about conventional regenerative braking strategy is shown as Fig. 14. The actual vehicle speed curve overlaps with the desired vehicle speed in Fig. 14(a). The difference between the vehicle speed and the wheel speed is small in Fig. 14(b), and the slip ratio is smaller than 0.05 in Fig. 14(c). The reason is the desired braking torque is small in the simulation scenario, and the slip ratio is in the line area. As depicted in Fig. 14(d), the desired braking torque is distributed to the front and rear

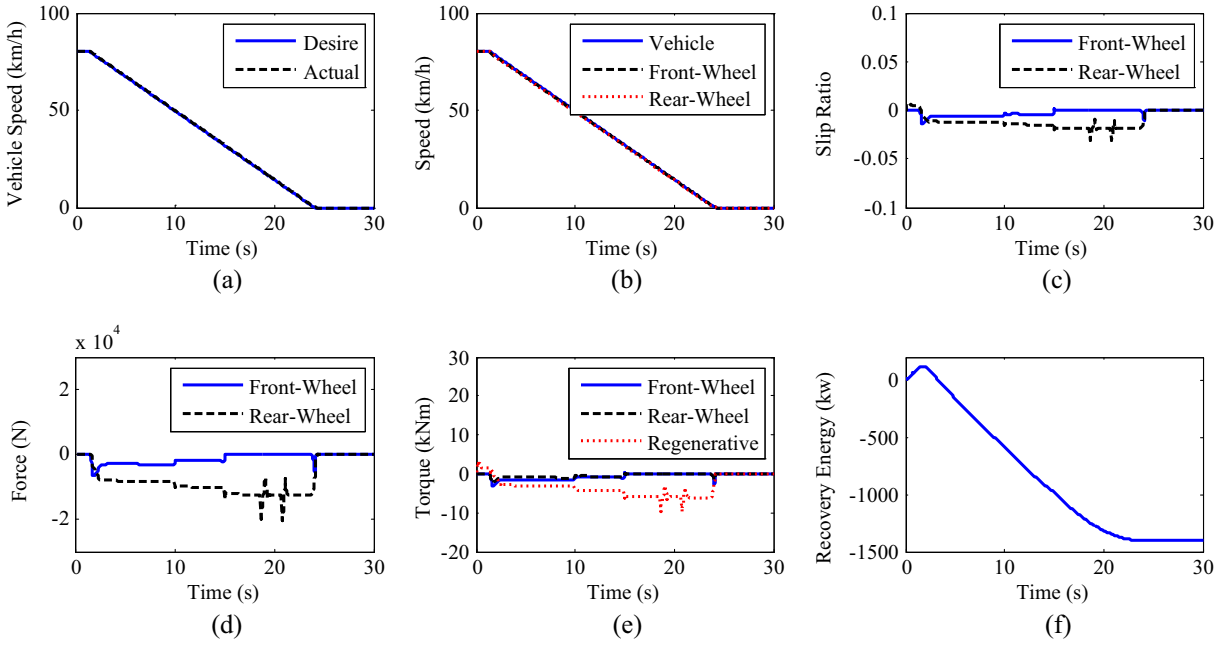

Fig. 15. The simulation result on general condition based on NMPC strategy.

wheel by a certain ratio, and the braking torque on the rear wheel is mainly provided by the motor. Gear-shifting operations are allowed in the general braking situation and the braking torque provided by the motor has a sharp corner in the gear-shifting process as shown in Fig. 14(e). The recovery energy is larger than that in the emergency braking situation as shown in Fig. 14(f).

4.2.2. The simulation on the general condition by modified NMPC strategy

The simulation result in the general braking process controlled by NMPC strategy is shown in Fig. 15. The actual vehicle speed curve also overlaps with the desired vehicle speed in Fig. 15(a), which denotes that the desired acceleration can be easily satisfied. The slip ratio is also in the linear area in Fig. 15(c). The slip ratio is so small that the wheel speed overlaps with the vehicle speed in Fig. 15(b). As shown in Fig. 15(d), the braking force on the front wheel is reducing and the braking force on the rear wheel is increasing after the gear-shifting process. As depicted in Fig. 15 (e), the regenerative braking torque in the earlier stage is the maximum regenerative braking torque that the motor can provide. With the gear reducing in the later stage, the regenerative braking torque that the motor can provide is increases and therefore the braking torque provided by the pneumatic braking system can be reduced. When the maximum regenerative braking torque that the motor can provide can satisfy the desired braking torque, the regenerative braking torque is equal to the desired braking torque. It is clear that the general braking process controlled by the proposed regenerative braking NMPC strategy can recover more braking energy in Fig. 15(f).

4.3. HIL test

HIL test enables experimental study for control algorithms via real time interaction between physical hardware and virtual simulations [31]. And the real-time calculation performance of the designed control strategy can be assessed in the HIL system, which is an effective tool in the ECU development process [32]. In this paper, the HIL test is carried out for the designed equivalent strategy in the fast NMPC implementation based on the xPC target environment, as shown in Fig. 16.

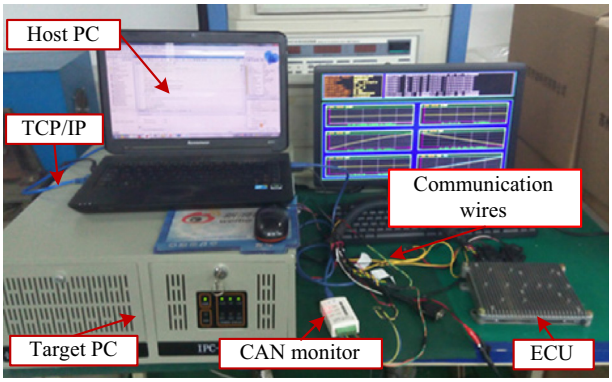

Fig. 16. The HIL platform.

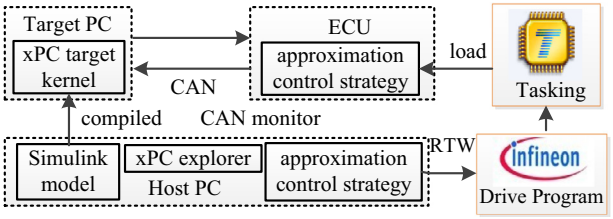

Fig. 17. The HIL system.

As shown in Fig. 17, the HIL system is composed of host PC, target PC, ECU, communication wires and CAN monitor. The host PC is used to control and monitor the test process. The target PC, an industrial personal computer (IPC), is employed to run the compiled model. An ECU is used as controller to run the equivalent control strategy coded by the real time workshop (RTW) tool of MATLAB. The communication between the host PC and the target PC is through TCP/IP protocol, and the information transmission

between target PC and ECU is performed through the controller area network (CAN). The CAN monitor is used to monitor and save the transmission information in the CAN buses. The time step of controller to send /receive the messages is 10 ms.

4.3.1. The HIL test about urgency braking situation

The HIL test result about urgency braking situation on the gravel road is shown in Fig. 18. The HIL test result is similar with that in the off-line simulation. There is a small difference between the desired vehicle speed and the actual vehicle speed in Fig. 18(a). The reasons are the same as that in the off-line simulation. The slip ratio is maintained within an acceptable range in Fig. 18(c). It denotes that the safety of vehicle is ensured in the HIL test. Compared with the off-line simulation, there are more vibration in the HIL test as shown in Fig. 18(d) and (e). The reason might be that the accuracy degree of the NP method is limited by the memory space of the controller, and the constraints of change rate of the braking torque is not included in the nominal off-line control strategy. The recovery energy is smaller than that in the off-line simulation. The reason may be that, to ensure the vehicle safety performance in the HIL test, the weight factor of the recovery energy is set to a small value.

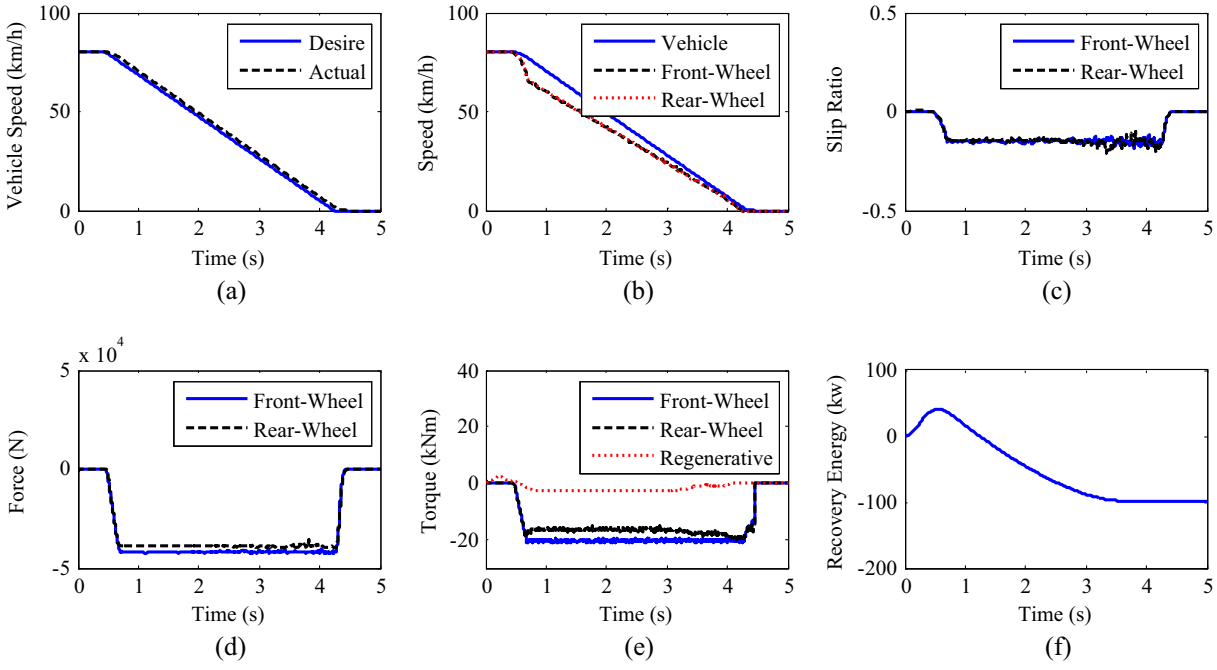

Fig. 18. The simulation result on urgency braking condition based on NMPC strategy in HIL test.

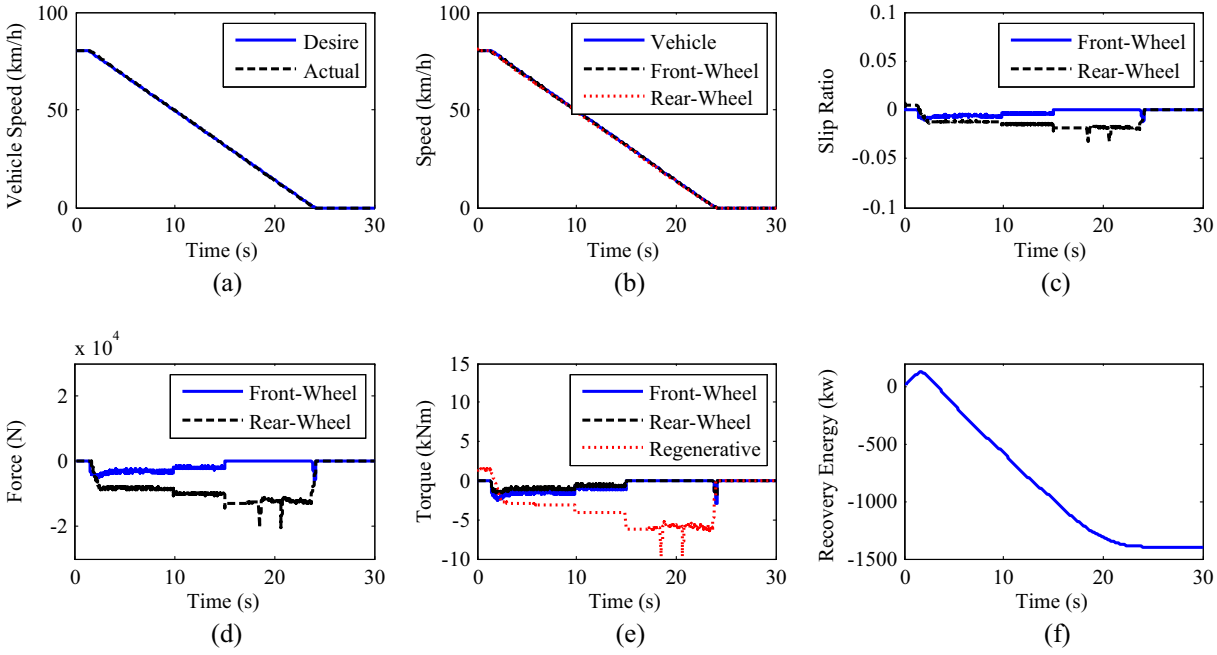

Fig. 19. The simulation result on general condition based on NMPC strategy in HIL test.

Table 4
HIL test result.

HIL TEST	Max slip ratio (front wheel)	Max slip ratio (rear wheel)	Whole braking energy (kJ)	Recovery braking energy (kJ)	Regeneration efficiency (%)
Emergency, gravel	0.1940	0.1933	3364.5	208.37	6.19
Emergency, ice	0.1937	0.1937	3283.7	406.17	12.37
Emergency, μ-jumped	0.4611	0.1903	3342.7	280.14	8.38
Conventional, PID	0.0136	0.0177	2923.5	1309.2	44.78
General, NMPC	0.0138	0.0314	2922.3	1523.4	52.13
Emergency, HIL test	0.1829	0.2061	3364.3	140.54	4.18
General, HIL test	0.0127	0.0322	2925.7	1522.9	52.05

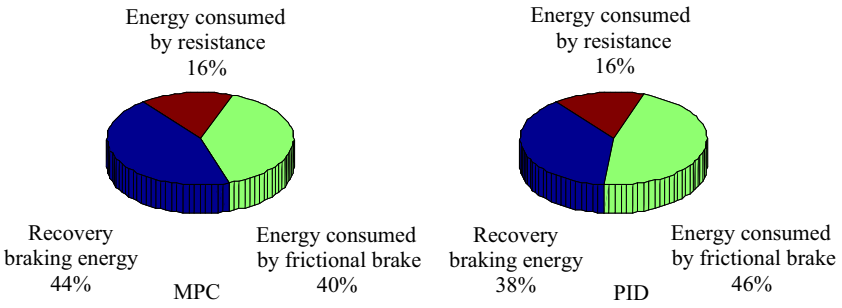

Fig. 20. Pie chart of the energy distribution in the general braking situation.

4.3.2. The HIL test result about general braking situation

The HIL test result about general braking situation on the gravel road, which is controlled by the fast NMPC strategy, is shown in Fig. 19. The actual vehicle speed overlaps with the desired vehicle speed in Fig. 19(a). The difference between the vehicle speed and the wheel speed is very small and the slip ratio is in the linear area. There are also some vibration as shown in Fig. 19(d) and (e). The vibration of the regenerative braking torque increases with reduced gear number, which can be due to the vibrations enhancement with higher gear ratios. As depicted in Fig. 19(f), the recovery energy is similar with that in the off-line simulation, which denotes that the fast NMPC strategy is effective to improve the regenerative energy in the HIL system.

As shown in Table 4, no max slip ratios of wheels reach to 1 in the simulation results about the emergency braking situation on various tire–road adhesion coefficient road, which shows that the proposed braking strategy can prevent the wheel from locking and ensure vehicle safety. The slip ratio in the simulation reaches to 0.46 when the tire–road adhesion coefficient changes, though it is beyond the rational region, it returns soon and the wheel is not locked. NMPC regenerative braking strategy is robust to changes on the road conditions. The recovery braking energy in the emergency braking situation, which is almost 208 kJ, is lower than that in the general braking situation, which is almost 1523 kJ. This is due to three main reasons: first, the safety of the vehicle is the main factor in the emergency situation; second, the desired braking torque is too large exceeding the motor torque limit; third, the gear-shifting operation is forbidden in the emergency braking situation. The simulation results about the general braking situation also show that the proposed NMPC strategy can recover more braking energy than the rule-based control strategy. The HIL test results are similar to the off-line simulation result, and the vehicle safety is ensured during the emergency braking test. Furthermore, the recovery braking energy in the HIL general braking test result is almost as same as that in the off-line simulation result, which is shown that the difference is just 0.5 kJ in Table 4. Thus the performance of the proposed strategy can be considered efficiently verified by the HIL test.

As depicted in Fig. 20, the recovery braking energy in the general braking process controlled by the proposed control strategy is 44%. Compared with the braking process controlled by the conventional control strategy, the recovery braking energy can improve 6% of the total braking energy and 17% of the recovery braking energy.

5. Conclusion

So as to balance the vehicle safety and braking energy recovery efficiency, this paper proposes an efficient energy recovery control strategy which is based on the MNMPC. A method for obtaining an optimal solution by modifying the PSO algorithm is also presented. Simulation and HIL test are carried out under different road conditions. The results show that the proposed strategy can ensure vehicle safety during emergency braking situation and improve the recovery energy almost 17% compared with the conventional rule-based strategy in the general braking situation. It is verified that the proposed strategy is effective due to the optimized distribution between pneumatic braking torque at the front and rear wheels respectively and the regenerative braking torque at the rear wheels using the NMPC method.

A further study could be performed with the application of the MNMPC strategy and the parameters used in the proposed strategy, which appropriately tuned could improve the algorithm performance.

Acknowledgments

The authors greatly appreciate the support from the National Natural Science Foundation of China National Funds for Excellent Yong Scholars (Grant No. 51422505) and the National Key Technology R&D Program of the Ministry of Science and Technology (Grant No. 2013BAG14B01).

References

[1] Hu X, Murgovski N, Johannesson LM, Egardt B. Comparison of three electrochemical energy buffers applied to a hybrid bus powertrain with simultaneous optimal sizing and energy management. IEEE Trans Intell Transp Syst 2014;15(3):1193–205.
[2] Çagatay Bayindir K, Gözüküçük MA, Teke A. A comprehensive overview of hybrid electric vehicle: powertrain configurations, powertrain control

techniques and electronic control units. Energy Convers Manage 2011;52 (2):1305–13.
[3] Wang L, Zhang Y. Hardware-in-the-loop simulation for the design and verification of the control system of a series–parallel hybrid electric city-bus. Simul Model Pract Theory 2012;25:148–62.
[4] Ehsani M, Gao Y, Butler KL. Application of electrically peaking hybrid (ELPH) propulsion system to a full size passenger car with simulated design verification. IEEE Trans Veh Technol 1999;48(6):1779–87.
[5] Kanarachos S, Alirezaei M, Jansen S, Maurice J. Control allocation for regenerative braking of electric vehicles with an electric motor at the front axle using the state-dependent Riccati equation control technique. Proc Inst Mech Eng D J Automot Eng 2014;228:129–43.
[6] Cao R, Mi C, Cheng M. Quantitative comparison of flux-switching permanent-magnet motors with interior permanent magnet motor for EV, HEV, and PHEV applications. IEEE Trans Magn 2012;48(8):2374–84.
[7] Vinot E, Trigui R. Optimal energy management of HEVs with hybrid storage system. Energy Convers Manage 2013;76:437–52.
[8] Xiong R, He H, Sun F, Zhao K. Online estimation of peak power capability of Li-ion batteries in electric vehicles by a hardware-in-loop approach. Energies 2012;5:1455–69.
[9] Zhang J, Li Y, Lv C, Yuan Y. New regenerative braking control strategy for rear-driven electrified minivans. Energy Convers Manage 2014;82:135–45.
[10] Gao Y, Ehsani M. Electronic braking system of EV and HEV—Integration of regenerative braking. Automatic braking force control and ABS. SAE technical paper 2001-01-2478; 2001.
[11] Zhang J, Lv C, Qiu M, Li Y, Sun D. Braking energy regeneration control of a fuel cell hybrid electric bus. Energy Convers Manage 2013;76:1117–24.
[12] He R, Zheng H, Zong C. Braking force distribution and coordinated control algorithm for hybrid electric bus based on EBS. SAE technical paper, 2014-01-1908; 2014.
[13] Kang M, Li L, Li H, Song J, Han Z. Coordinated vehicle traction control based on engine torque and brake pressure under complicated road conditions. Veh Syst Dyn 2012;50(9):1473–94.
[14] Bera TK, Bhattacharya K, Samantaray AK. Bond graph model-based evaluation of a sliding mode controller for a combined regenerative and antilock braking system. Proc Inst Mech Eng D J Automot Eng 2010;225:918–34.
[15] Kim D, Kim J, Hwang S, Kim H. Optimal brake torque distribution for a four-wheel-drive hybrid electric vehicle stability enhancement. Proc Inst Mech Eng D J Automot Eng 2007;221:1357–66.
[16] Zhang J, Song B, Cui S, Ren D. Fuzzy logic approach to regenerative braking system. Intell Human Mach Syst Cybernet 2009;1:451–4.
[17] Xu G, Li W, Xu K, Song Z. An intelligent regenerative braking strategy for electric vehicles. Energies 2011;4:1461–77.
[18] Huang X, Wang J. Model predictive regenerative braking control for lightweight electric vehicles with in-wheel motors. Proc Inst Mech Eng D J Automot Eng 2012;226:1220–32.
[19] Liu W, He H, Guo H, Sun F. Control research for hybrid compound braking based on an uncertainty predictive model. ITEC Asia-Pacific; 2014.
[20] Wang B, Huang X, Wang J, Guo X, Zhu X. A robust wheel slip control design for in-wheel-motor-driven electric vehicles with hydraulic and regenerative braking systems. Am Cont Conf (ACC) 2014.
[21] Zhang H, Zhang X, Wang J. Robust gain-scheduling energy-to-peak control of vehicle lateral dynamics stabilization. Veh Syst Dyn 2014;52(3):309–40.
[22] Pacejka HB, Bakker E. The magic formula tyre model. Veh Syst Dyn 1992;21 (suppl):1–18.
[23] Li S, Li K, Rajamani R, Wang J. Model predictive multi-objective vehicular adaptive cruise control. IEEE Trans Cont Syst Technol 2011;19(3):556–66.
[24] Chan C. Modified particle swarm optimization algorithm for multi-objective optimization design of hybrid journal bearings. ASME J Tribol 2015;137:021101.
[25] Marini F, Walczak B. Particle swarm optimization (PSO). A tutorial. Chemomet Intell Lab Syst 2015. http://dx.doi.org/10.1016/j.chemolab.2015.08.020.
[26] Bageshwar VL, Garrard WL, Rajamani R. Model predictive control of transitional maneuvers for adaptive cruise control vehicles. IEEE Trans Veh Technol 2004;53(5):1573–85.
[27] Zheng C, Xu G, Xu K, Pan Z, Liang Q. An energy management approach of hybrid vehicles using traffic preview information for energy saving. Energy Convers Manage 2015;105:462–70.
[28] Canale M, Fagiano L, Milanese M. Set membership approximation theory for fast implementation of model predictive control laws. Automatica 2009;45 (1):45–54.
[29] Canale M, Fagiano L, Razza V. Approximate NMPC for vehicle stability: design, implementation and SIL testing. Cont Eng Pract 2010;18:630–9.
[30] Fukunaga K. Introduction to statistical pattern recognition. 2nd ed. San Diego: Academic Press; 1990.
[31] Petersheim M, Brennan S. Scaling of hybrid-electric vehicle powertrain components for hardware-in-the-loop simulation. Mechatronics 2009;19 (7):1078–90.
[32] Conti R, Meli E, Ridolfi A, Rindi A. An innovative hardware in the loop architecture of the analysis of railway braking under degraded adhesion conditions through roller-rigs. Mechatronics 2014;24(2):139–50.